Supplement of

Oxygenated organic molecules produced by low-NO_x photooxidation of aromatic compounds and their contributions to secondary organic aerosol

Xi Cheng[1], Yong Jie Li[2], Yan Zheng[1], Keren Liao[1], Tong Zhu[1], Chunxiang Ye[1], Xinghua Qiu[1], Theodore K. Koenig[1], Yanli Ge[1], Qi Chen[1]

[1]State Key Joint Laboratory of Environmental Simulation and Pollution Control, BIC-ESAT and IJRC, College of Environmental Sciences and Engineering, Peking University, Beijing, China

[2]Department of Civil and Environmental Engineering, Department of Ocean Science and Technology, and Centre for Regional Oceans, Faculty of Science and Technology, University of Macau, Taipa, Macau, China

Correspondence: Qi Chen (qichenpku@pku.edu.cn) and Yong Jie Li (yongjieli@um.edu.mo)

S1. Methods

Loss rate of OOMs

Losses of oxygenated organic molecules (OOMs) in an oxidation flow reactor (OFR) include the loss to the OFR walls (k_{wall}, s^{-1}), the loss to aerosol particles presented in the OFR (i.e., the condensation sink, CS, s^{-1}), and the loss to non-condensable products due to continuous reaction with OH (k_{OHloss}, s^{-1}) (Palm et al., 2016). According to the method described by Brune (2019) and Huang et al. (2018), k_{wall} of 0.0023-0.0028 s^{-1} are used in our experiments. The CS was calculated using the data from scanning mobility particle sizer (SMPS), the average CS for the experiments herein is 0.02-0.07 s^{-1}. The average k_{OHloss} are then calculated as 0.02-0.04 s^{-1} using the approach of Palm et al. (2016). More detailed descriptions could be found in our previous study (Cheng et al., 2021).

VBS parametrization

The volatility of gaseous OOMs was estimated using a volatility parameterization method (Mohr et al., 2019). The saturation concentrations (C^*) at 300 K for individual organic compounds are given by:

$$\log_{10}C^* = (n_0 - n_C) \times b_C - n_O \times b_O - 2\left(\frac{n_C \times n_O}{n_C + n_O}\right) \times b_{CO} \quad \text{(S1)}$$

where $n_0 = 25$, $b_C = 0.475$, $b_O = 0.2$, $b_{CO} = 0.9$, and n_C and n_O are the number of carbon and oxygen atoms in the compound, respectively (Donahue et al., 2011).

The saturation concentrations of compounds at ambient temperature were obtained by:

$$\log_{10}C^*(T) = \log_{10}C^*(300K) + \frac{\Delta H_{vap}}{R\ln(10)}\left(\frac{1}{300} - \frac{1}{T}\right) \quad \text{(S2)}$$

where the evaporation enthalpy ΔH_{vap} can be linked to saturation concentration $\log_{10}C^*(300K)$ via:

$$\Delta H_{vap}\ [kJ\ mol^{-1}] = -11\log_{10}C^*(300K) + 129 \quad \text{(S3)}$$

The OOMs were then grouped into different bins within a volatility basis set (VBS) based on C^* (Donahue et al., 2006), and further classified as: ultralow volatility organic compound (ULVOC, $\log C^* \leq -9.5$); extremely low volatility organic compound (ELVOC, $-9.5 < \log C^* \leq -4.5$); low volatility organic compound (LVOC, $-4.5 < \log C^* \leq -0.5$); semi-volatile organic compound (SVOC, $-0.5 < \log C^* \leq 2.5$); intermediate volatility organic compound (IVOC, $2.5 < \log C^* \leq 6.5$) (Shrivastava et al., 2017; Bianchi et al., 2019; Schervish and Donahue, 2020).

Aerosol growth model

To evaluate the contribution of OOMs to secondary organic aerosols (SOA) through condensation, we used the aerosol growth model to calculate the net condensation flux of the observed OOMs (Tröstl et al., 2016), as follows:

$$\phi_p = N_p \times \sigma_p \times s_p \times F_p \quad \text{(S4)}$$

Combining the first three terms, then the modified equation is:

$$\phi_p = N_p \pi D_p^2 \times \frac{(D_p + D_i)^2}{D_p^2}\frac{v_i}{4}\alpha_i\beta_i \times F_p \quad \text{(S5)}$$

with N_p being the particle number concentration, D_p the particle diameter, D_i the vapour diameter, v_i the center of mass velocity for particle and vapor, α_i the accommodation coefficient, β_i the correction factor for the transition regime. F_p is

the driving force of condensation, $F_p = C^v - X_p \Upsilon_p K_p C^*$, where C^v is the vapour (OOMs) concentration, C^* is the saturation concentration, X_p is the mass fraction of OOMs of each VBS bin in the condensed phase, and Υ_p is the mass-based activity coefficient in the condensed phase (assuming $\Upsilon_p = 1$ as in ideal organic solution). The Kelvin term, $K_p = \exp(\frac{4\sigma M}{RT\rho D_p})$, which is related to the surface tension σ, molar weight M, and density ρ.

When the organic vapours in the gas and condensed phases reach equilibrium (F_p is zero), equilibrium partitioning theory is used to describe the condensation and evaporation of the organics onto or from particle surface (Pankow, 1994). The fraction of species i in the condensed phase is defined as:

$$f_i = \frac{1}{1 + C^*/C_{OA}} \quad \text{(S6)}$$

where C_{OA} is the concentration of organic aerosol in the condensed phase.

S2. General mechanism of OH-initiated chemistry of aromatic VOCs

The OH-initiated chemistry of aromatic volatile organic compounds (VOCs) mainly proceeds via addition to the aromatic ring to generate OH-aromatic adducts. If there are alkyl substitutions on the aromatic rings, reactions can also proceed via H-atom abstraction for normally ≤10% probability (Jenkin et al., 2003). The alkyl radicals (R) formed either way react with O_2 and form a variety of RO_2 radicals, which undergo the following reaction channels under low-NO_x conditions: (1) bimolecular reaction route (reacting with HO_2 or RO_2 radicals) to form termination products or alkoxy radicals (RO), (2) phenolic route through HO_2 elimination, and (3) bicyclic intermediate route through cyclization (Jenkin et al., 2003; Nishino et al., 2012). The new alkyl (R) radical from the important pathway (3) can be converted to a new RO_2 radical by incorporating an O_2 molecule, forming a host of monomeric and dimeric OOMs via reactions R-S1 to R-S7 (Cheng et al., 2021; Garmash et al., 2020). Among these reactions, R-S1 is the autoxidation pathway that incorporates more and more oxygen atoms into the products while forming peroxide groups (-OOH) by internal H-shift; R-S2, R-S3, and R-S5 are termination reactions that lead to various monomeric products with different functional groups; R-S4 and R-S6 are the RO pathway between reactions of RO_2 and HO_2 or RO_2, and subsequent isomerization of RO might result in a new RO_2; R-S7 is the accretion reaction that leads to dimer formation.

Autoxidation pathway:

$$RO_2 \rightarrow \bullet QOOH;\ \bullet QOOH + O_2 \rightarrow R(OOH)O_2 \quad \text{(R-S1)}$$

General RO_2 pathways:

$$RO_2 + HO_2 \rightarrow ROOH + O_2 \text{ (hydroperoxide channel)} \quad \text{(R-S2)}$$

$$RO_2 + HO_2 \rightarrow ROH + O_3 \text{ (hydroxyl channel)} \quad \text{(R-S3)}$$

$$RO_2 + HO_2 \rightarrow RO + OH + O_2 \text{ (alkoxy radical channel)} \quad \text{(R-S4)}$$

$$RO_2 + R'O_2 \rightarrow ROH + R'HC{=}O + O_2 \text{ (hydroxyl/carbonyl channel)} \quad \text{(R-S5)}$$

$$RO_2 + R'O_2 \rightarrow RO + R'O + O_2 \text{ (alkoxy radical channel)} \quad \text{(R-S6)}$$

$$RO_2 + R'O_2 \rightarrow ROOR' + O_2 \text{ (dimer channel)} \quad \text{(R-S7)}$$

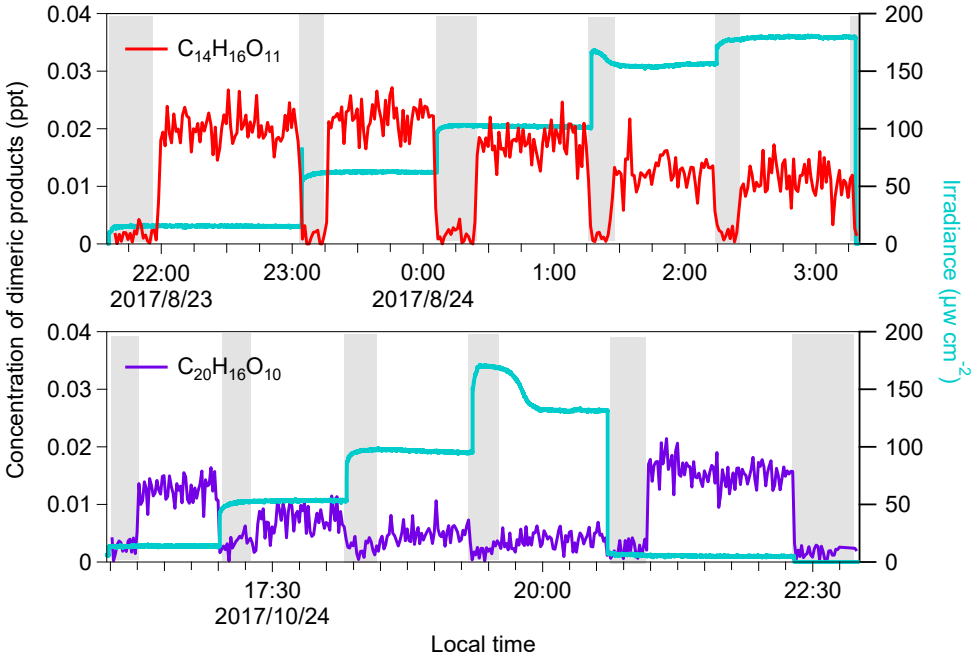

Figure S1. Time series of experimental conditions (irradiance in the OFR) and the example dimeric products from toluene and naphthalene oxidation. The grey shaded area represents "background" periods without VOC injection.

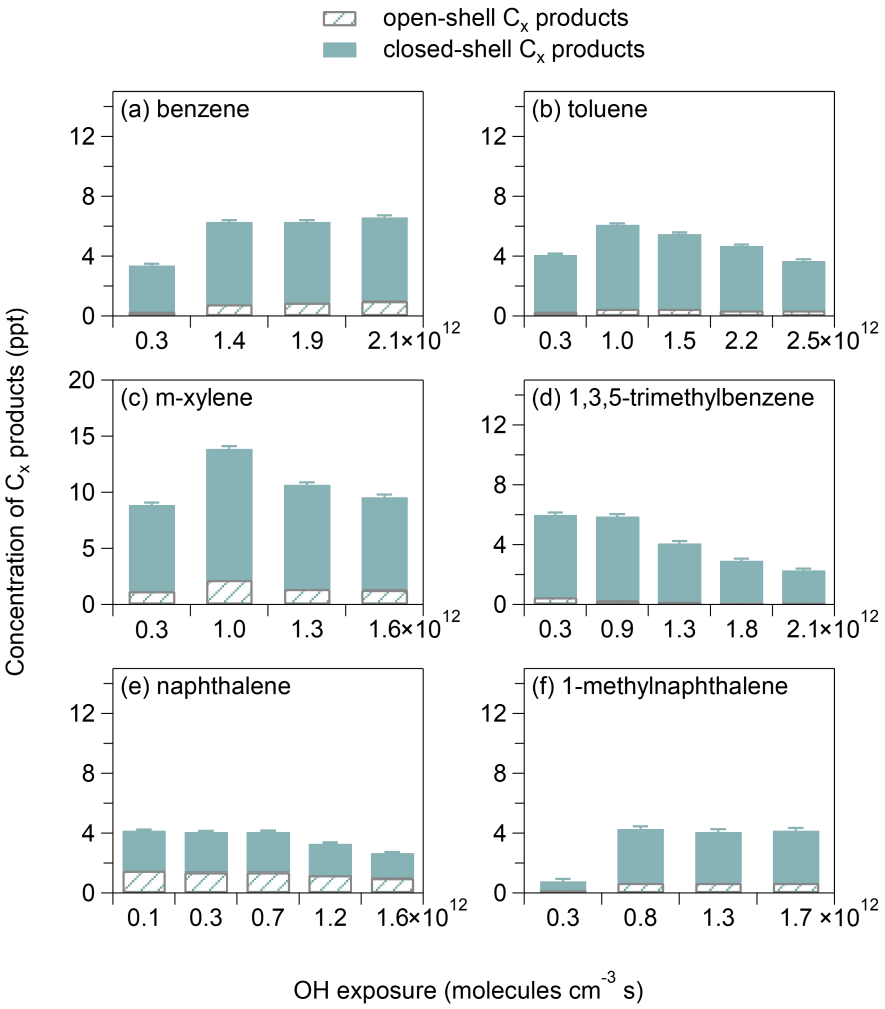

Figure S2. Concentrations of C_x products formed from the oxidation of **(a)** benzene, **(b)** toluene, **(c)** m-xylene, **(d)** 1,3,5-trimethylbenzene, **(e)** naphthalene and **(f)** 1-methylnaphthalene at different OH exposure. C_x products consist of open-shell and closed-shell monomers.

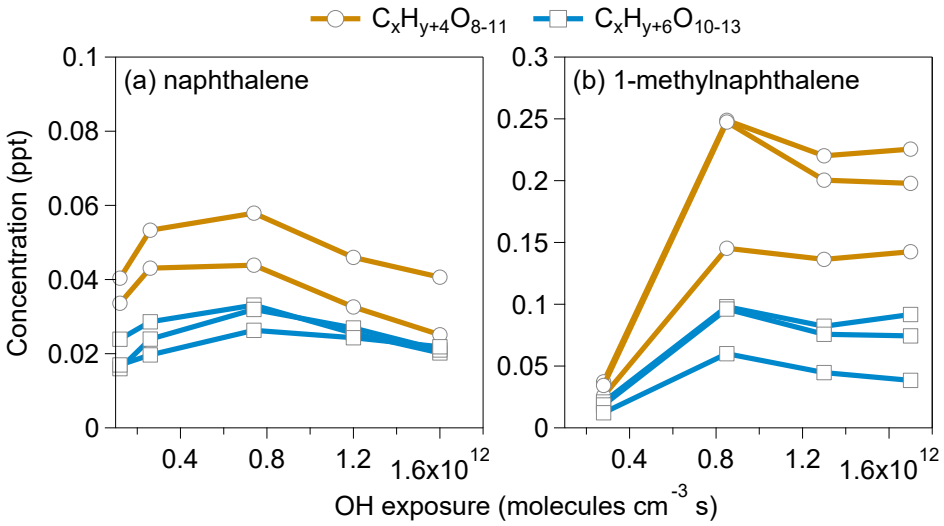

Figure S3. Concentrations of C_xH_{y+4}- and C_xH_{y+6}-series monomeric products formed from the oxidation of **(a)** naphthalene and **(b)** 1-methylnaphthalene at different OH exposure.

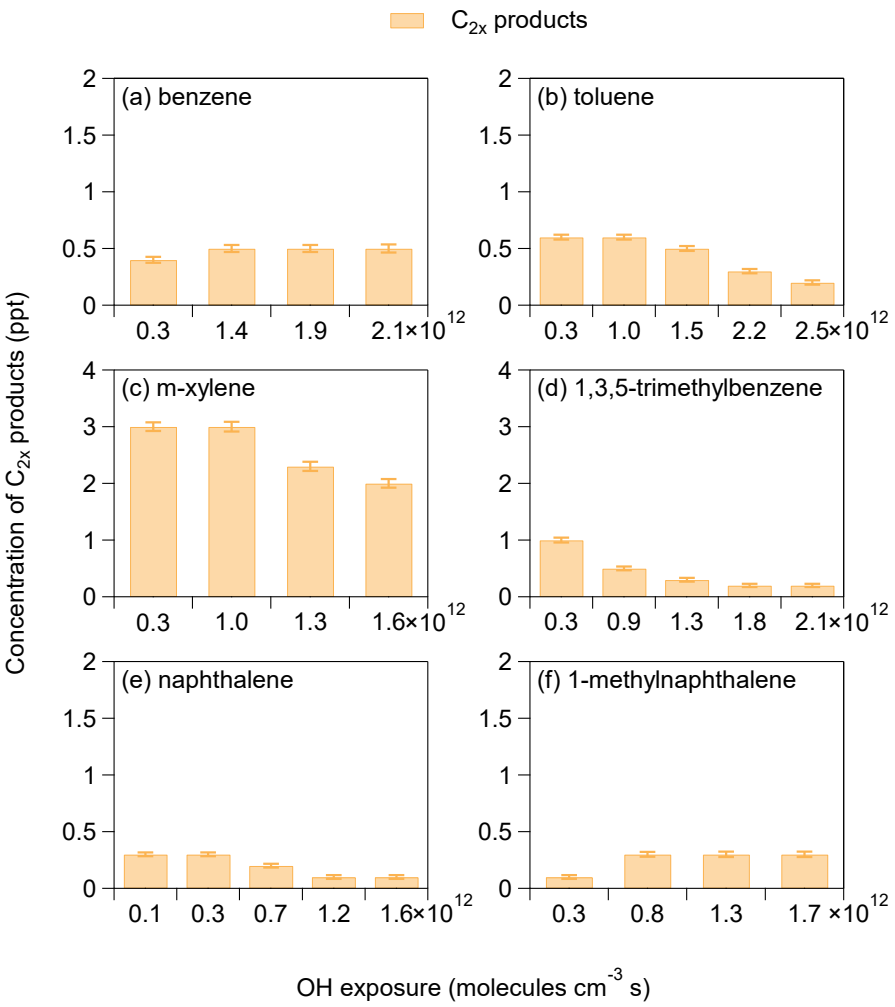

Figure S4. Concentrations of C_{2x} products formed from the oxidation of **(a)** benzene, **(b)** toluene, **(c)** m-xylene, **(d)** 1,3,5-trimethylbenzene, **(e)** naphthalene and **(f)** 1-methylnaphthalene at different OH exposure.

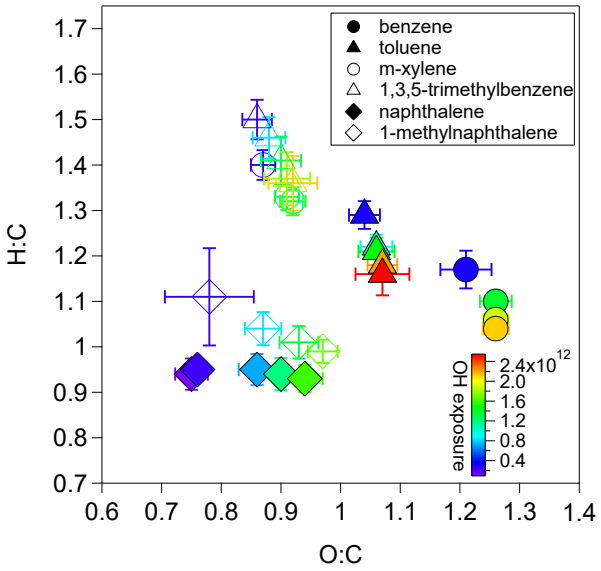

Figure S5. H:C and O:C ratios of gaseous OOMs formed from photooxidation of benzene, toluene, m-xylene, 1,3,5-trimethylbenzene, naphthalene and 1-methylnaphthalene at different OH exposure.

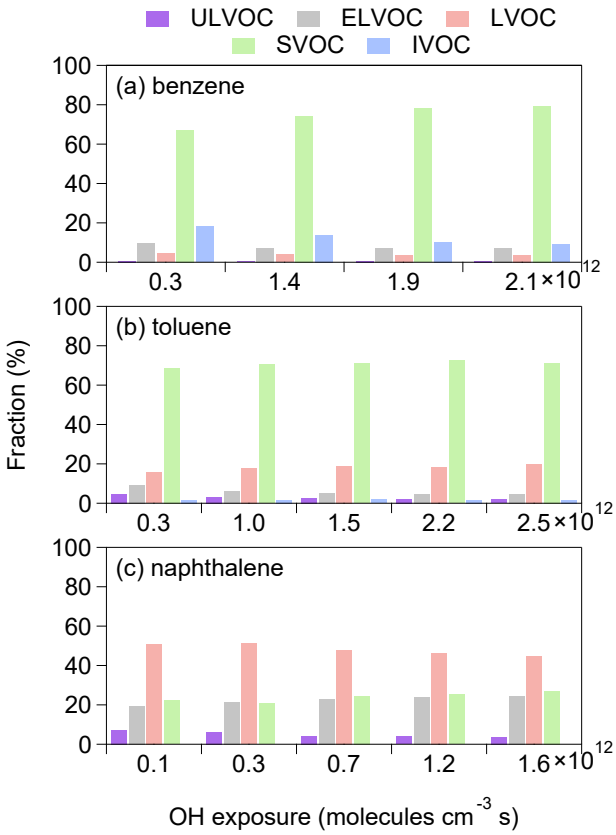

Figure S6. Concentration fractions of gaseous OOMs formed from the oxidation of **(a)** benzene, **(b)** toluene and **(c)** naphthalene at different OH exposure. OOMs are classified as five volatility classes: ULVOC, ELVOC, LVOC, SVOC, and IVOC.

Table S1. Parts of the peak list for benzene (C_6H_6) oxidation products shown in Fig. 1a.

Category	Formula	*m/z* (Th)	Fraction of fitted signals
$C_{2\text{-}5}$ monomeric products	$C_3H_4O_5$	181.99	9.2%
	$C_4H_4O_5$	193.99	14.3%
	$C_4H_6O_5$	196.01	2.1%
	$C_5H_4O_5$	205.99	6.6%
	$C_5H_6O_5$	208.01	1.5%
	$C_4H_4O_6$	209.99	2.6%
	$C_5H_4O_6$	221.99	7.8%
C_6 monomeric products	$C_6H_6O_5$	220.01	3.0%
	$C_6H_7O_5$	221.02	0.1%
	$C_6H_8O_5$	222.03	0.4%
	$C_6H_{10}O_5$	224.04	0.8%
	$C_6H_5O_6$	235.00	0.6%
	$C_6H_6O_6$	236.00	3.1%
	$C_6H_7O_6$	237.01	0.2%
	$C_6H_8O_6$	238.02	1.8%
	$C_6H_{10}O_6$	240.04	0.2%
	$C_6H_5O_7$	250.99	1.0%
	$C_6H_6O_7$	252.00	2.9%
	$C_6H_7O_7$	253.01	0.4%
	$C_6H_8O_7$	254.02	2.4%
	$C_6H_9O_7$	255.02	0.1%
	$C_6H_{10}O_7$	256.03	0.5%
	$C_6H_5O_8$	266.99	0.3%
	$C_6H_6O_8$	267.99	1.3%
	$C_6H_7O_8$	269.00	0.2%
	$C_6H_8O_8$	270.01	1.9%
	$C_6H_9O_8$	271.02	0.1%
	$C_6H_{10}O_8$	272.03	0.9%
	$C_6H_5O_9$	282.98	0.3%
	$C_6H_6O_9$	283.99	0.6%
	$C_6H_7O_9$	285.00	0.9%
	$C_6H_8O_9$	286.01	1.1%
	$C_6H_9O_9$	287.01	0.3%
	$C_6H_{10}O_9$	288.02	0.4%
	$C_6H_5O_{10}$	298.98	0.1%
	$C_6H_6O_{10}$	299.98	0.3%
	$C_6H_7O_{10}$	300.99	0.6%
	$C_6H_8O_{10}$	302.00	0.5%
	$C_6H_{10}O_{10}$	304.02	0.2%
$C_{10\text{-}11}$ dimeric products	$C_{11}H_{14}O_9$	352.05	0.04%
	$C_{10}H_{10}O_{12}$	384.01	0.1%
	$C_{10}H_{12}O_{12}$	386.02	0.04%
C_{12} dimeric products	$C_{12}H_{14}O_8$	348.06	0.05%
	$C_{12}H_{14}O_9$	364.05	0.07%
	$C_{12}H_{10}O_{10}$	376.02	0.13%
	$C_{12}H_{12}O_{10}$	378.03	0.13%
	$C_{12}H_{14}O_{10}$	380.05	0.13%
	$C_{12}H_{16}O_{10}$	382.06	0.06%
	$C_{12}H_{10}O_{11}$	392.01	0.05%
	$C_{12}H_{12}O_{11}$	394.03	0.11%
	$C_{12}H_{14}O_{11}$	396.04	0.16%
	$C_{12}H_{16}O_{11}$	398.06	0.10%
	$C_{12}H_{10}O_{12}$	408.01	0.15%
	$C_{12}H_{12}O_{12}$	410.02	0.14%
	$C_{12}H_{14}O_{12}$	412.04	0.15%
	$C_{12}H_{16}O_{12}$	414.05	0.09%
	$C_{12}H_{10}O_{13}$	424.00	0.05%
	$C_{12}H_{12}O_{13}$	426.02	0.17%
	$C_{12}H_{14}O_{13}$	428.03	0.15%
	$C_{12}H_{16}O_{13}$	430.05	0.09%

$C_{12}H_{10}O_{14}$	440.00	0.06%
$C_{12}H_{12}O_{14}$	442.01	0.06%
$C_{12}H_{14}O_{14}$	444.03	0.1%
$C_{12}H_{16}O_{14}$	446.04	0.05%

Table S2. Parts of the peak list for toluene (C_7H_8) oxidation products shown in Fig. 1b.

Category	Formula	*m/z* (Th)	Fraction of total fitted signals
C_{2-6} monomeric products	$C_3H_4O_5$	181.99	2.4%
	$C_4H_4O_5$	193.99	5.9%
	$C_4H_6O_5$	196.01	9.5%
	$C_5H_4O_5$	205.99	3.5%
	$C_5H_6O_5$	208.01	5.7%
	$C_5H_4O_6$	221.99	7.2%
C_7 monomeric products	$C_7H_8O_5$	234.03	1.3%
	$C_7H_9O_5$	235.03	0.1%
	$C_7H_{10}O_5$	236.04	0.6%
	$C_7H_7O_6$	249.01	0.2%
	$C_7H_8O_6$	250.02	3.8%
	$C_7H_9O_6$	251.03	0.2%
	$C_7H_{10}O_6$	252.04	2.1%
	$C_7H_{12}O_6$	254.05	0.1%
	$C_7H_7O_7$	265.01	0.2%
	$C_7H_8O_7$	266.02	2.6%
	$C_7H_9O_7$	267.02	0.5%
	$C_7H_{10}O_7$	268.03	3.0%
	$C_7H_{11}O_7$	269.04	0.1%
	$C_7H_{12}O_7$	270.05	0.7%
	$C_7H_7O_8$	281.00	0.2%
	$C_7H_8O_8$	282.01	1.6%
	$C_7H_9O_8$	283.02	0.1%
	$C_7H_{10}O_8$	284.03	2.0%
	$C_7H_{11}O_8$	285.03	0.2%
	$C_7H_{12}O_8$	286.04	1.0%
	$C_7H_8O_9$	298.01	0.4%
	$C_7H_9O_9$	299.01	1.0%
	$C_7H_{10}O_9$	300.02	1.3%
	$C_7H_{11}O_9$	301.03	0.2%
	$C_7H_{12}O_9$	302.04	0.4%
	$C_7H_8O_{10}$	314.00	0.3%
	$C_7H_9O_{10}$	315.01	0.4%
	$C_7H_{10}O_{10}$	316.02	0.4%
	$C_7H_{12}O_{10}$	318.03	0.2%
C_{10-13} dimeric products	$C_{10}H_{10}O_9$	336.02	0.1%
	$C_{12}H_{10}O_8$	344.03	0.03%
	$C_{13}H_{12}O_9$	374.04	0.02%
	$C_{13}H_{14}O_{10}$	392.05	0.03%
C_{14} dimeric products	$C_{14}H_{18}O_8$	376.09	0.03%
	$C_{14}H_{16}O_9$	390.07	0.04%
	$C_{14}H_{18}O_9$	392.08	0.03%
	$C_{14}H_{20}O_9$	394.10	0.01%
	$C_{14}H_{16}O_{10}$	406.06	0.06%
	$C_{14}H_{18}O_{10}$	408.08	0.1%
	$C_{14}H_{20}O_{10}$	410.09	0.04%
	$C_{14}H_{16}O_{11}$	422.06	0.08%
	$C_{14}H_{18}O_{11}$	424.07	0.08%
	$C_{14}H_{20}O_{11}$	426.09	0.11%
	$C_{14}H_{16}O_{12}$	438.05	0.07%
	$C_{14}H_{18}O_{12}$	440.07	0.13%
	$C_{14}H_{20}O_{12}$	442.08	0.07%
	$C_{14}H_{16}O_{13}$	454.05	0.07%
	$C_{14}H_{18}O_{13}$	456.06	0.1%
	$C_{14}H_{20}O_{13}$	458.08	0.08%
	$C_{14}H_{16}O_{14}$	470.04	0.05%
	$C_{14}H_{18}O_{14}$	472.06	0.07%
	$C_{14}H_{20}O_{14}$	474.07	0.05%

Table S3. Parts of the peak list for m-xylene (C_8H_{10}) oxidation products shown in Fig. 1c.

Category	Formula	*m/z* (Th)	Fraction of total fitted signals
$C_{2\text{-}7}$ monomeric products	$C_3H_4O_5$	181.99	0.4%
	$C_4H_4O_5$	193.99	0.7%
	$C_5H_4O_5$	205.99	0.2%
	$C_5H_6O_5$	208.01	1.5%
	$C_4H_4O_6$	209.99	0.3%
	$C_5H_8O_5$	210.03	0.1%
	$C_4H_6O_6$	212.00	0.3%
	$C_5H_6O_6$	224.00	2.5%
C_8 monomeric products	$C_8H_{10}O_5$	248.04	0.06%
	$C_8H_{11}O_5$	249.05	0.05%
	$C_8H_{12}O_5$	250.06	0.2%
	$C_8H_8O_6$	262.02	0.5%
	$C_8H_{10}O_6$	264.04	2.3%
	$C_8H_{11}O_6$	265.04	0.7%
	$C_8H_{12}O_6$	266.05	1.5%
	$C_8H_{13}O_6$	267.06	0.1%
	$C_8H_{14}O_6$	268.07	0.2%
	$C_8H_8O_7$	278.02	1.6%
	$C_8H_9O_7$	279.02	0.1%
	$C_8H_{10}O_7$	280.03	8.6%
	$C_8H_{11}O_7$	281.04	0.9%
	$C_8H_{12}O_7$	282.05	4.4%
	$C_8H_{13}O_7$	283.05	0.4%
	$C_8H_{14}O_7$	284.06	1.8%
	$C_8H_8O_8$	294.01	0.6%
	$C_8H_9O_8$	295.02	0.1%
	$C_8H_{10}O_8$	296.03	6.4%
	$C_8H_{11}O_8$	297.03	0.9%
	$C_8H_{12}O_8$	298.04	4.6%
	$C_8H_{13}O_8$	299.05	0.9%
	$C_8H_{14}O_8$	300.06	3.5%
	$C_8H_{10}O_9$	312.02	2.6%
	$C_8H_{11}O_9$	313.03	1.0%
	$C_8H_{12}O_9$	314.04	4.4%
	$C_8H_{13}O_9$	315.04	0.6%
	$C_8H_{14}O_9$	316.05	2.3%
	$C_8H_9O_{10}$	327.01	0.1%
	$C_8H_{10}O_{10}$	328.02	0.5%
	$C_8H_{11}O_{10}$	329.02	0.1%
	$C_8H_{12}O_{10}$	330.03	1.0%
	$C_8H_{13}O_{10}$	331.04	0.5%
	$C_8H_{14}O_{10}$	332.05	0.6%
$C_{10\text{-}15}$ dimeric products	$C_{14}H_8O_5$	318.03	0.14%
	$C_{13}H_{10}O_6$	324.04	0.11%
	$C_{11}H_{14}O_8$	336.06	0.07%
	$C_{14}H_{12}O_6$	338.05	0.16%
	$C_{13}H_{10}O_8$	356.03	0.06%
	$C_{14}H_{20}O_{10}$	410.09	0.18%
C_{16} dimeric products	$C_{16}H_{18}O_7$	384.09	0.11%
	$C_{16}H_{18}O_8$	400.09	0.1%
	$C_{16}H_{18}O_9$	416.08	0.08%
	$C_{16}H_{20}O_9$	418.10	0.06%
	$C_{16}H_{22}O_9$	420.11	0.11%
	$C_{16}H_{18}O_{10}$	432.08	0.08%
	$C_{16}H_{20}O_{10}$	434.09	0.14%
	$C_{16}H_{22}O_{10}$	436.11	0.3%
	$C_{16}H_{24}O_{10}$	438.13	0.28%
	$C_{16}H_{20}O_{11}$	450.09	0.26%
	$C_{16}H_{22}O_{11}$	452.10	0.37%
	$C_{16}H_{24}O_{11}$	454.12	0.48%

$C_{16}H_{20}O_{12}$	466.08	0.33%
$C_{16}H_{22}O_{12}$	468.10	0.54%
$C_{16}H_{24}O_{12}$	470.12	0.47%
$C_{16}H_{20}O_{13}$	482.08	0.3%
$C_{16}H_{22}O_{13}$	484.09	0.46%
$C_{16}H_{24}O_{13}$	486.11	0.47%
$C_{16}H_{20}O_{14}$	498.07	0.19%
$C_{16}H_{22}O_{14}$	500.09	0.32%
$C_{16}H_{24}O_{14}$	502.10	0.27%

Table S4. Parts of the peak list for 1,3,5-trimethylbenzene (C_9H_{12}) oxidation products shown in Fig. 1d.

Category	Formula	*m/z* (Th)	Fraction of total fitted signals
$C_{2\text{-}8}$ monomeric products	$C_3H_4O_5$	181.99	0.2%
	$C_4H_4O_5$	193.99	0.7%
	$C_5H_4O_5$	205.99	0.1%
	$C_5H_6O_5$	208.01	0.6%
	$C_4H_4O_6$	209.99	0.3%
	$C_5H_8O_5$	210.03	0.1%
	$C_4H_6O_6$	212.00	0.5%
	$C_6H_6O_5$	220.01	0.3%
	$C_5H_4O_6$	221.99	0.5%
	$C_5H_6O_6$	224.00	0.8%
	$C_6H_6O_6$	236.00	0.9%
	$C_6H_8O_6$	238.02	0.9%
	$C_7H_{10}O_6$	252.04	0.8%
	$C_8H_{10}O_6$	264.04	1.5%
	$C_7H_8O_7$	266.02	0.7%
	$C_8H_{10}O_7$	280.03	3.1%
	$C_8H_{12}O_7$	282.05	1.8%
C_9 monomeric products	$C_9H_{12}O_5$	262.06	0.2%
	$C_9H_{13}O_5$	263.06	0.1%
	$C_9H_{12}O_6$	278.05	2.7%
	$C_9H_{14}O_6$	280.07	1.4%
	$C_9H_{16}O_6$	282.08	0.2%
	$C_9H_{10}O_7$	292.03	0.7%
	$C_9H_{12}O_7$	294.05	4.4%
	$C_9H_{13}O_7$	295.05	0.13%
	$C_9H_{14}O_7$	296.06	17.5%
	$C_9H_{15}O_7$	297.07	1.6%
	$C_9H_{16}O_7$	298.08	3.4%
	$C_9H_{10}O_8$	308.03	0.5%
	$C_9H_{12}O_8$	310.04	6.0%
	$C_9H_{13}O_8$	311.05	0.3%
	$C_9H_{14}O_8$	312.06	4.3%
	$C_9H_{15}O_8$	313.07	0.5%
	$C_9H_{16}O_8$	314.07	3.7%
	$C_9H_{10}O_9$	324.02	0.6%
	$C_9H_{12}O_9$	326.04	2.3%
	$C_9H_{13}O_9$	327.04	0.4%
	$C_9H_{14}O_9$	328.05	4.1%
	$C_9H_{15}O_9$	329.06	0.4%
	$C_9H_{16}O_9$	330.07	2.8%
	$C_9H_{10}O_{10}$	340.02	0.1%
	$C_9H_{12}O_{10}$	342.03	0.9%
	$C_9H_{13}O_{10}$	343.04	0.7%
	$C_9H_{14}O_{10}$	344.05	1.4%
	$C_9H_{15}O_{10}$	345.05	0.5%
	$C_9H_{16}O_{10}$	346.06	0.8%
$C_{10\text{-}17}$ dimeric products	$C_{11}H_{18}O_8$	340.09	0.09%
	$C_{12}H_{18}O_8$	352.09	0.13%
	$C_{11}H_{16}O_9$	354.07	0.05%
	$C_{14}H_{14}O_7$	356.06	0.05%
	$C_{12}H_{10}O_{12}$	408.01	0.12%
C_{18} dimeric products	$C_{18}H_{24}O_{10}$	462.13	0.09%
	$C_{18}H_{26}O_{10}$	464.14	0.19%
	$C_{18}H_{28}O_{10}$	466.16	0.08%
	$C_{18}H_{24}O_{11}$	478.12	0.11%
	$C_{18}H_{26}O_{11}$	480.14	0.13%
	$C_{18}H_{28}O_{11}$	482.15	0.16%
	$C_{18}H_{24}O_{12}$	494.12	0.23%
	$C_{18}H_{26}O_{12}$	496.13	0.37%
	$C_{18}H_{28}O_{12}$	498.15	0.22%

$C_{18}H_{24}O_{13}$	510.11	0.1%
$C_{18}H_{26}O_{13}$	512.13	0.23%
$C_{18}H_{28}O_{13}$	514.14	0.18%
$C_{18}H_{24}O_{14}$	526.10	0.12%
$C_{18}H_{26}O_{14}$	528.12	0.18%
$C_{18}H_{28}O_{14}$	530.14	0.17%

Table S5. Parts of the peak list for naphthalene ($C_{10}H_8$) oxidation products shown in Fig. 1e.

Category	Formula	*m/z* (Th)	Fraction of total fitted signals
$C_{2\text{-}9}$ monomeric products	$C_3H_4O_5$	181.99	8.9%
	$C_4H_4O_5$	193.99	9.3%
	$C_4H_6O_5$	196.01	1.7%
	$C_5H_4O_5$	205.99	3.7%
	$C_5H_6O_5$	208.01	1.0%
	$C_4H_4O_6$	209.99	2.3%
	$C_6H_6O_5$	220.01	1.0%
	$C_5H_4O_6$	221.99	2.5%
	$C_5H_8O_6$	226.02	5.6%
	$C_7H_6O_6$	248.00	0.6%
	$C_9H_8O_7$	290.02	2.1%
C_{10} monomeric products	$C_{10}H_6O_5$	268.01	0.6%
	$C_{10}H_7O_5$	269.02	0.2%
	$C_{10}H_8O_5$	270.03	2.8%
	$C_{10}H_9O_5$	271.03	0.4%
	$C_{10}H_{10}O_5$	272.04	0.5%
	$C_{10}H_{11}O_5$	273.05	0.1%
	$C_{10}H_{12}O_5$	274.06	0.2%
	$C_{10}H_{13}O_5$	275.06	0.1%
	$C_{10}H_6O_6$	284.00	0.5%
	$C_{10}H_7O_6$	285.01	0.1%
	$C_{10}H_8O_6$	286.02	2.9%
	$C_{10}H_9O_6$	287.03	0.3%
	$C_{10}H_{10}O_6$	288.04	0.9%
	$C_{10}H_{11}O_6$	289.04	0.5%
	$C_{10}H_{12}O_6$	290.05	0.3%
	$C_{10}H_{13}O_6$	291.06	0.2%
	$C_{10}H_{14}O_6$	292.07	0.1%
	$C_{10}H_6O_7$	300.00	0.1%
	$C_{10}H_7O_7$	301.01	0.3%
	$C_{10}H_8O_7$	302.02	1.8%
	$C_{10}H_9O_7$	303.02	1.0%
	$C_{10}H_{10}O_7$	304.03	1.0%
	$C_{10}H_{11}O_7$	305.04	0.3%
	$C_{10}H_{12}O_7$	306.05	0.2%
	$C_{10}H_{13}O_7$	307.05	0.1%
	$C_{10}H_{14}O_7$	308.06	0.1%
	$C_{10}H_6O_8$	315.99	0.1%
	$C_{10}H_7O_8$	317.00	0.3%
	$C_{10}H_8O_8$	318.01	0.5%
	$C_{10}H_9O_8$	319.02	1.1%
	$C_{10}H_{10}O_8$	320.03	1.0%
	$C_{10}H_{11}O_8$	321.03	0.3%
	$C_{10}H_{12}O_8$	322.04	0.3%
	$C_{10}H_{13}O_8$	323.05	0.1%
	$C_{10}H_{14}O_8$	324.06	0.1%
	$C_{10}H_6O_9$	331.99	0.1%
	$C_{10}H_7O_9$	333.00	0.1%
	$C_{10}H_8O_9$	334.01	0.4%
	$C_{10}H_9O_9$	335.01	0.3%
	$C_{10}H_{10}O_9$	336.02	0.6%
	$C_{10}H_{11}O_9$	337.03	0.3%
	$C_{10}H_{12}O_9$	338.04	0.5%
	$C_{10}H_{13}O_9$	339.04	0.1%
	$C_{10}H_{14}O_9$	340.05	0.1%
	$C_{10}H_7O_{10}$	348.99	0.4%
	$C_{10}H_8O_{10}$	350.00	0.2%
	$C_{10}H_9O_{10}$	351.01	0.5%
	$C_{10}H_{10}O_{10}$	352.02	0.7%
	$C_{10}H_{11}O_{10}$	353.02	0.4%
	$C_{10}H_{12}O_{10}$	354.03	0.6%

	$C_{10}H_7O_{11}$	364.99	0.2%
	$C_{10}H_8O_{11}$	366.00	0.2%
	$C_{10}H_9O_{11}$	367.00	0.2%
	$C_{10}H_{10}O_{11}$	368.01	0.4%
	$C_{10}H_{11}O_{11}$	369.02	0.2%
	$C_{10}H_{12}O_{11}$	370.03	0.6%
	$C_{10}H_{13}O_{11}$	371.03	0.2%
	$C_{10}H_{14}O_{11}$	372.04	0.3%
	$C_{10}H_7O_{12}$	380.98	0.1%
	$C_{10}H_8O_{12}$	381.99	0.1%
	$C_{10}H_9O_{12}$	383.00	0.1%
	$C_{10}H_{10}O_{12}$	384.01	0.2%
	$C_{10}H_{11}O_{12}$	385.01	0.2%
	$C_{10}H_{12}O_{12}$	386.02	0.4%
	$C_{10}H_{13}O_{12}$	387.03	0.1%
	$C_{10}H_{14}O_{12}$	388.04	0.2%
$C_{11\text{-}19}$ dimeric products	$C_{11}H_{14}O_{13}$	416.03	0.02%
	$C_{14}H_{14}O_{12}$	436.04	0.04%
	$C_{18}H_{12}O_{12}$	482.02	0.02%
C_{20} dimeric products	$C_{20}H_{14}O_8$	444.06	0.01%
	$C_{20}H_{16}O_8$	446.07	0.02%
	$C_{20}H_{16}O_9$	462.07	0.03%
	$C_{20}H_{18}O_9$	464.08	0.01%
	$C_{20}H_{14}O_{10}$	476.05	0.02%
	$C_{20}H_{16}O_{10}$	478.06	0.03%
	$C_{20}H_{18}O_{10}$	480.08	0.02%
	$C_{20}H_{14}O_{11}$	492.04	0.02%
	$C_{20}H_{16}O_{11}$	494.06	0.03%
	$C_{20}H_{18}O_{11}$	496.07	0.03%
	$C_{20}H_{20}O_{11}$	498.09	0.02%
	$C_{20}H_{14}O_{12}$	508.04	0.02%
	$C_{20}H_{16}O_{12}$	510.05	0.01%
	$C_{20}H_{18}O_{12}$	512.07	0.02%
	$C_{20}H_{20}O_{12}$	514.08	0.03%
	$C_{20}H_{22}O_{12}$	516.10	0.01%
	$C_{20}H_{20}O_{13}$	530.08	0.01%
	$C_{20}H_{18}O_{14}$	544.06	0.02%
	$C_{20}H_{20}O_{14}$	546.07	0.03%

Table S6. Parts of the peak list for 1-methylnaphthalene ($C_{11}H_{10}$) oxidation products shown in Fig. 1f.

Category	Formula	*m/z* (Th)	Fraction of total fitted signals
$C_{2\text{-}10}$ monomeric products	$C_3H_4O_5$	181.99	4.1%
	$C_4H_4O_5$	193.99	2.7%
	$C_4H_6O_5$	196.01	0.4%
	$C_5H_4O_5$	205.99	0.8%
	$C_5H_6O_5$	208.01	1.0%
	$C_4H_6O_6$	212.00	0.6%
	$C_5H_4O_6$	221.99	4.0%
	$C_5H_6O_6$	224.00	3.0%
	$C_6H_6O_6$	236.00	1.9%
	$C_5H_6O_7$	240.00	1.2%
	$C_6H_6O_7$	252.00	2.8%
C_{11} monomeric products	$C_{11}H_{10}O_5$	284.04	0.4%
	$C_{11}H_{11}O_5$	285.05	0.05
	$C_{11}H_{12}O_5$	286.06	0.1%
	$C_{11}H_8O_6$	298.02	0.7%
	$C_{11}H_9O_6$	299.03	0.1%
	$C_{11}H_{10}O_6$	300.04	0.7%
	$C_{11}H_{11}O_6$	301.04	0.1%
	$C_{11}H_{12}O_6$	302.05	0.2%
	$C_{11}H_8O_7$	314.02	0.4%
	$C_{11}H_9O_7$	315.02	0.2%
	$C_{11}H_{10}O_7$	316.03	0.6%
	$C_{11}H_{11}O_7$	317.04	0.1%
	$C_{11}H_{12}O_7$	318.05	0.4%
	$C_{11}H_{14}O_7$	320.06	0.2%
	$C_{11}H_8O_8$	330.01	0.4%
	$C_{11}H_9O_8$	331.02	0.1%
	$C_{11}H_{10}O_8$	332.03	0.8%
	$C_{11}H_{11}O_8$	333.03	0.2%
	$C_{11}H_{12}O_8$	334.04	1.0%
	$C_{11}H_{13}O_8$	335.05	0.1%
	$C_{11}H_{14}O_8$	336.06	0.5%
	$C_{11}H_8O_9$	346.01	0.3%
	$C_{11}H_9O_9$	347.01	0.1%
	$C_{11}H_{10}O_9$	348.02	0.9%
	$C_{11}H_{11}O_9$	349.03	0.1%
	$C_{11}H_{12}O_9$	350.04	1.6%
	$C_{11}H_{13}O_9$	351.04	0.2%
	$C_{11}H_{14}O_9$	352.05	1.1%
	$C_{11}H_{16}O_9$	354.07	0.2%
	$C_{11}H_8O_{10}$	362.00	0.4%
	$C_{11}H_9O_{10}$	363.01	0.2%
	$C_{11}H_{10}O_{10}$	364.02	1.0%
	$C_{11}H_{11}O_{10}$	365.02	0.1%
	$C_{11}H_{12}O_{10}$	366.03	2.1%
	$C_{11}H_{13}O_{10}$	367.04	0.2%
	$C_{11}H_{14}O_{10}$	368.05	1.9%
	$C_{11}H_{16}O_{10}$	370.06	0.5%
	$C_{11}H_{10}O_{11}$	380.01	0.8%
	$C_{11}H_{11}O_{11}$	381.02	0.1%
	$C_{11}H_{12}O_{11}$	382.03	1.8%
	$C_{11}H_{13}O_{11}$	383.03	0.2%
	$C_{11}H_{14}O_{11}$	384.04	1.8%
	$C_{11}H_{16}O_{11}$	386.06	0.7%
	$C_{11}H_{10}O_{12}$	396.01	0.4%
	$C_{11}H_{11}O_{12}$	397.01	0.2%
	$C_{11}H_{12}O_{12}$	398.02	1.3%
	$C_{11}H_{13}O_{12}$	399.03	0.2%
	$C_{11}H_{14}O_{12}$	400.04	1.3%
	$C_{11}H_{16}O_{12}$	402.05	0.6%
	$C_{11}H_{10}O_{13}$	412.00	0.2%

	$C_{11}H_{11}O_{13}$	413.01	0.1%
	$C_{11}H_{12}O_{13}$	414.02	0.6%
	$C_{11}H_{13}O_{13}$	415.02	0.2%
	$C_{11}H_{14}O_{13}$	416.03	0.7%
	$C_{11}H_{16}O_{13}$	418.05	0.4%
	$C_{11}H_{10}O_{14}$	428.00	0.1%
	$C_{11}H_{12}O_{14}$	430.01	0.3%
	$C_{11}H_{13}O_{14}$	431.02	0.1%
	$C_{11}H_{14}O_{14}$	432.03	0.4%
	$C_{11}H_{16}O_{14}$	434.04	0.2%
$C_{12\text{-}21}$ dimeric products	$C_{13}H_{18}O_4$	300.11	0.04%
	$C_{20}H_{10}O_5$	392.04	0.02%
C_{22} dimeric products	$C_{22}H_{18}O_9$	488.08	0.02%
	$C_{22}H_{22}O_9$	492.11	0.02%
	$C_{22}H_{18}O_{10}$	504.08	0.02%
	$C_{22}H_{20}O_{10}$	506.09	0.02%
	$C_{22}H_{22}O_{10}$	508.11	0.02%
	$C_{22}H_{24}O_{10}$	510.13	0.02%
	$C_{22}H_{18}O_{11}$	520.07	0.04%
	$C_{22}H_{20}O_{11}$	522.09	0.03%
	$C_{22}H_{22}O_{11}$	524.10	0.04%
	$C_{22}H_{24}O_{11}$	526.12	0.02%
	$C_{22}H_{20}O_{12}$	538.08	0.04%
	$C_{22}H_{22}O_{12}$	540.10	0.05%
	$C_{22}H_{24}O_{12}$	542.12	0.04%
	$C_{22}H_{18}O_{13}$	552.06	0.03%
	$C_{22}H_{20}O_{13}$	554.08	0.03%
	$C_{22}H_{22}O_{13}$	556.09	0.04%
	$C_{22}H_{24}O_{13}$	558.11	0.04%
	$C_{22}H_{18}O_{14}$	568.06	0.01%
	$C_{22}H_{20}O_{14}$	570.07	0.06%
	$C_{22}H_{22}O_{14}$	572.09	0.05%
	$C_{22}H_{24}O_{14}$	574.10	0.04%

Table S7. Fraction of the major C_x-series monomers, and C_{2x}-series dimers selected from Tables S1-S6.

	benzene (%)	toluene (%)	m-xylene (%)	1,3,5-trimethylbenzene (%)	naphthalene (%)	1-methylnaphthalene (%)
$C_xH_{y+1}O_5$	0.1	0.1	0.05	0.1	0.4	0.05
$C_xH_{y+1}O_6$	0.2	0.2	0.7	/	0.3	0.1
$C_xH_{y+1}O_7$	0.4	0.5	0.9	0.13	1	0.1
$C_xH_{y+1}O_8$	0.2	0.1	0.9	0.3	1.1	0.2
$C_xH_{y+1}O_9$	0.9	1	1	0.4	0.3	0.1
$C_{2x}H_{2y}O_{10\text{-}14}$	0.6	0.3	1.2	0.7	0.1	0.2
$C_{2x}H_{2y+2}O_{10\text{-}14}$	0.7	0.5	2.0	1.1	0.1	0.2
$C_{2x}H_{2y+4}O_{10\text{-}14}$	0.4	0.4	2.0	0.8	0.1	0.2

References

Bianchi, F., Kurten, T., Riva, M., Mohr, C., Rissanen, M. P., Roldin, P., Berndt, T., Crounse, J. D., Wennberg, P. O., Mentel, T. F., Wildt, J., Junninen, H., Jokinen, T., Kulmala, M., Worsnop, D. R., Thornton, J. A., Donahue, N., Kjaergaard, H. G., and Ehn, M.: Highly oxygenated organic molecules (HOM) from gas-phase autoxidation involving peroxy radicals: a key contributor to atmospheric aerosol, Chem. Rev., 119, 3472-3509, https://doi.org/10.1021/acs.chemrev.8b00395, 2019.

Brune, W. H.: The chamber wall index for gas-wall interactions in atmospheric environmental enclosures, Environ. Sci. Technol., 53, 3645-3652, https://doi.org/10.1021/acs.est.8b06260, 2019.

Cheng, X., Chen, Q., Li, Y., Zheng, Y., Liao, K., and Huang, G.: Highly oxygenated organic molecules produced by the oxidation of benzene and toluene in a wide range of OH exposure and NOx conditions, Atmos. Chem. Phys., 21, 12005-12019, https://doi.org/10.5194/acp-21-12005-2021, 2021.

Donahue, N. M., Epstein, S. A., Pandis, S. N., and Robinson, A. L.: A two-dimensional volatility basis set: 1. organic-aerosol mixing thermodynamics, Atmos. Chem. Phys., 11, 3303-3318, https://doi.org/10.5194/acp-11-3303-2011, 2011.

Donahue, N. M., Robinson, A. L., Stanier, C. O., and Pandis, S. N.: Coupled partitioning, dilution, and chemical aging of semivolatile organics, Environ. Sci. Technol., 40, 2635-2643, https://doi.org/10.1021/es052297c, 2006.

Garmash, O., Rissanen, M. P., Pullinen, I., Schmitt, S., Kausiala, O., Tillmann, R., Zhao, D., Percival, C., Bannan, T. J., Priestley, M., Hallquist, Å. M., Kleist, E., Kiendler-Scharr, A., Hallquist, M., Berndt, T., McFiggans, G., Wildt, J., Mentel, T. F., and Ehn, M.: Multi-generation OH oxidation as a source for highly oxygenated organic molecules from aromatics, Atmos. Chem. Phys., 20, 515-537, https://doi.org/10.5194/acp-20-515-2020, 2020.

Huang, Y. L., Zhao, R., Charan, S. M., Kenseth, C. M., Zhang, X., and Seinfeld, J. H.: Unified theory of vapor-wall mass transport in teflon-walled environmental chambers, Environ. Sci. Technol., 52, 2134-2142, https://doi.org/10.1021/acs.est.7b05575, 2018.

Jenkin, M. E., Saunders, S. M., Wagner, V., and Pilling, M. J.: Protocol for the development of the Master Chemical Mechanism, MCM v3 (Part B): tropospheric degradation of aromatic volatile organic compounds, Atmos. Chem. Phys., 3, 181-193, https://doi.org/10.5194/acp-3-181-2003, 2003.

Mohr, C., Thornton, J. A., Heitto, A., Lopez-Hilfiker, F. D., Lutz, A., Riipinen, I., Hong, J., Donahue, N. M., Hallquist, M., Petaja, T., Kulmala, M., and Yli-Juuti, T.: Molecular identification of organic vapors driving atmospheric nanoparticle growth, Nat. Commun., 10, https://doi.org/10.1038/s41467-019-12473-2, 2019.

Nishino, N., Arey, J., and Atkinson, R.: 2-Formylcinnamaldehyde formation yield from the OH radical-initiated reaction of naphthalene: effect of NO2 concentration, Environ. Sci. Technol., 46, 8198-8204, https://doi.org/10.1021/es301865t, 2012.

Palm, B. B., Campuzano-Jost, P., Ortega, A. M., Day, D. A., Kaser, L., Jud, W., Karl, T., Hansel, A., Hunter, J. F., Cross, E. S., Kroll, J. H., Peng, Z., Brune, W. H., and Jimenez, J. L.: In situ secondary organic aerosol formation from ambient pine forest air using an oxidation flow reactor, Atmos. Chem. Phys., 16, 2943-2970, https://doi.org/10.5194/acp-16-2943-2016, 2016.

Pankow, J. F.: An absorption model of gas/particle partitioning of organic compounds in the atmosphere, Atmos. Environ., 28, 185-188, https://doi.org/10.1016/1352-2310(94)90093-0, 1994.

Schervish, M., and Donahue, N. M.: Peroxy radical chemistry and the volatility basis set, Atmos. Chem. Phys., 20, 1183-1199, https://doi.org/10.5194/acp-20-1183-2020, 2020.

Shrivastava, M., Cappa, C. D., Fan, J., Goldstein, A. H., Guenther, A. B., Jimenez, J. L., Kuang, C., Laskin, A., Martin, S. T., Ng, N. L., Petaja, T., Pierce, J. R., Rasch, P. J., Roldin, P., Seinfeld, J. H., Shilling, J., Smith, J. N., Thornton, J. A.,

Volkamer, R., Wang, J., Worsnop, D. R., Zaveri, R. A., Zelenyuk, A., and Zhang, Q.: Recent advances in understanding secondary organic aerosol: implications for global climate forcing, Rev. Geophys., 55, 509-559, https://doi.org/10.1002/2016rg000540, 2017.

Tröstl, J., Chuang, W. K., Gordon, H., Heinritzi, M., Yan, C., Molteni, U., Ahlm, L., Frege, C., Bianchi, F., Wagner, R., Simon, M., Lehtipalo, K., Williamson, C., Craven, J. S., Duplissy, J., Adamov, A., Almeida, J., Bernhammer, A.-K., Breitenlechner, M., Brilke, S., Dias, A., Ehrhart, S., Flagan, R. C., Franchin, A., Fuchs, C., Guida, R., Gysel, M., Hansel, A., Hoyle, C. R., Jokinen, T., Junninen, H., Kangasluoma, J., Keskinen, H., Kim, J., Krapf, M., Kürten, A., Laaksonen, A., Lawler, M., Leiminger, M., Mathot, S., Möhler, O., Nieminen, T., Onnela, A., Petäjä, T., Piel, F. M., Miettinen, P., Rissanen, M. P., Rondo, L., Sarnela, N., Schobesberger, S., Sengupta, K., Sipilä, M., Smith, J. N., Steiner, G., Tomè, A., Virtanen, A., Wagner, A. C., Weingartner, E., Wimmer, D., Winkler, P. M., Ye, P., Carslaw, K. S., Curtius, J., Dommen, J., Kirkby, J., Kulmala, M., Riipinen, I., Worsnop, D. R., Donahue, N. M., and Baltensperger, U.: The role of low-volatility organic compounds in initial particle growth in the atmosphere, Nature, 533, 527-531, https://doi.org/10.1038/nature18271, 2016.